Research Article | Vol. 24, No. 14 | 11 Jul 2016 | OPTICS EXPRESS 16191

Optics EXPRESS

Single mode criterion - a benchmark figure to optimize the performance of nonlinear fibers

MARIO CHEMNITZ[1,*] AND MARKUS A. SCHMIDT[1,2]

[1] *Leibniz Institute of Photonic Technology, Albert-Einstein-Str. 9, 07745 Jena, Germany*
[2] *Otto Schott Institute of Material Research (OSIM), Friedrich Schiller University of Jena, Fraunhoferstrasse 6, 07743 Jena, Germany*
[*] *mario.chemnitz@ipht-jena.de*

Abstract: Optical fibers with sub-wavelength cores are promising systems for efficient nonlinear light generation. Here we reveal that the single-mode criterion represents a convenient design tool to optimize the performance of nonlinear fibers circumventing intense numerical calculations. We introduce a quasi-analytic expression for the nonlinear coefficient allowing us to investigate its behavior over a large parameter range. The study is independent of the actual value of the material nonlinearity and shows the fundamental dependencies of the nonlinear coefficient on wavelength, refractive index and core diameter, elucidated by detailed case studies of fused silica and chalcogenide tapers and hybrid fibers.

OCIS codes: (060.2280) Fiber design and fabrication; (060.4370) Nonlinear optics, fibers; (160.2290) Fiber materials; (190.4400) Nonlinear optics, materials; (220.0220) Optical design and fabrication; (230.4320) Nonlinear optical devices.

References and links

1. T. Gottschall, T. Meyer, M. Baumgartl, C. Jauregui, M. Schmitt, J. Popp, J. Limpert, and A. Tünnermann, "Fiber-based light sources for biomedical applications of coherent anti-Stokes Raman scattering microscopy," Laser Photonics Rev. **9**, 435–451 (2015).
2. A. Matveev, C. G. Parthey, K. Predehl, J. Alnis, A. Beyer, R. Holzwarth, T. Udem, T. Wilken, N. Kolachevsky, M. Abgrall, D. Rovera, C. Salomon, P. Laurent, G. Grosche, O. Terra, T. Legero, H. Schnatz, S. Weyers, B. Altschul, and T. W. Hänsch, "Precision measurement of the hydrogen 1S-2S frequency via a 920-km fiber link," Phys. Rev. Lett. **110**, 1–5 (2013).
3. K. Goda and B. Jalali, "Dispersive Fourier transformation for fast continuous single-shot measurements," Nat. Photonics **7**, 102–112 (2013).
4. X. Jiang, N. Y. Joly, M. A. Finger, F. Babic, G. K. L. Wong, J. C. Travers, and P. S. J. Russell, "Deep-ultraviolet to mid-infrared supercontinuum generated in solid-core ZBLAN photonic crystal fibre," Nat. Photonics **9**, 133–139 (2015).
5. C. R. Petersen, U. Møller, I. Kubat, B. Zhou, S. Dupont, J. Ramsay, T. Benson, S. Sujecki, N. Abdel-Moneim, Z. Tang, D. Furniss, A. Seddon, and O. Bang, "Mid-IR supercontinuum covering the molecular fingerprint region from 2μm to 13μm using ultra-high NA chalcogenide step-index fibre," Nat. Photonics **8**, 830–834 (2014).
6. J. M. Dudley, G. Genty, and S. Coen, "Supercontinuum generation in photonic crystal fiber," Rev. Mod. Phys. **78**, 1135–1184 (2006).
7. F. Biancalana, T. X. Tran, S. Stark, M. A. Schmidt, and P. S. J. Russell, "Emergence of geometrical optical nonlinearities in photonic crystal fiber nanowires," Phys. Rev. Lett. **105**, 093904 (2010).
8. N. Granzow, S. P. Stark, M. A. Schmidt, A. S. Tverjanovich, L. Wondraczek, and P. S. Russell, "Supercontinuum generation in chalcogenide-silica step-index fibers," Opt. Express **19**, 21003–21010 (2011).
9. N. Granzow, M. A. Schmidt, W. Chang, L. Wang, Q. Coulombier, J. Troles, P. Toupin, I. Hartl, K. F. Lee, M. E. Fermann, L. Wondraczek, and P. S. Russell, "Mid-infrared supercontinuum generation in As_2S_3-silica nano-spike step-index waveguide," Opt. Express **21**, 10969–10977 (2013).
10. K. F. Lee, N. Granzow, M. A. Schmidt, W. Chang, L. Wang, Q. Coulombier, J. Troles, N. Leindecker, K. L. Vodopyanov, P. G. Schunemann, M. E. Fermann, P. S. J. Russell, and I. Hartl, "Midinfrared frequency combs from coherent supercontinuum in chalcogenide and optical parametric oscillation," Opt. Lett. **39**, 2056–2059 (2014).
11. D.-I. Yeom, E. C. Mägi, M. R. E. Lamont, M. A. F. Roelens, L. Fu, and B. J. Eggleton, "Low-threshold supercontinuum generation in highly nonlinear chalcogenide nanowires," Opt. Lett. **33**, 660–662 (2008).
12. E. Lepine, Z. Yang, Y. Gueguen, J. Troles, X.-H. Zhang, B. Bureau, C. Boussard-Pledel, J.-C. Sangleboeuf, and P. Lucas, "Optical microfabrication of tapers in low-loss chalcogenide fibers," J. Opt. Soc. Am. B **27**, 966–971

#263230 http://dx.doi.org/10.1364/OE.24.016191
Journal © 2016 Received 14 Apr 2016; revised 27 May 2016; accepted 30 May 2016; published 8 Jul 2016
Corrected: 11 July 2016

Optics EXPRESS

(2010).
13. M. Artiglia and G. Coppa, "Mode field diameter measurements in single-mode optical fibers," J. Lightwave Technol. **7**, 1139–1152 (1989).
14. K. Petermann, "Microbending loss in monomode fibres," Electron. Lett. **12**, 107–109 (1976).
15. P. S. J. Russell, "Photonic crystal fibers," **299**, 358–362 (2003).
16. G. P. Agrawal, *Nonlinear fiber optics, 5th Ed.* (Academic Press. 2013).
17. M. Foster, K. Moll, and A. Gaeta, "Optimal waveguide dimensions for nonlinear interactions," Opt. Express **12**, 2880–2887 (2004).
18. A. W. Snyder and J. D. Love, *Optical Waveguide Theory* (Chapman and Hall, 1983).
19. S. Afshar V. and T. M. Monro, "A full vectorial model for pulse propagation in emerging waveguides with subwavelength structures part I: Kerr nonlinearity," Opt. Express **17**, 2298–2318 (2009).
20. T. A. Birks, W. J. Wadsworth, and P. S. J. Russell, "Supercontinuum generation in tapered fibers." Opt. Lett. **25**, 1415–1417 (2000).
21. I. Kubat, C. Agger, P. Moselund, and O. Bang, "Mid-infrared supercontinuum generation to 4.5 μm in uniform and tapered ZBLAN step-index fibers by direct pumping at 1064 or 1550 nm," J. Opt. Soc. Am. B **30**, 2743–2757 (2013).
22. S. Wang, C. Jain, L. Wondraczek, K. Wondraczek, J. Kobelke, J. Troles, C. Caillaud, and M. a. Schmidt, "Non-Newtonian flow of an ultralow-melting chalcogenide liquid in strongly confined geometry," Appl. Phys. Lett. **106**, 201908 (2015).
23. C. Jain, B. P. Rodrigues, T. Wieduwilt, J. Kobelke, L. Wondraczek, and M. A. Schmidt, "Silver metaphosphate glass wires inside silica fibers a new approach for hybrid optical fibers," Opt. Express **24**, 3258–3267 (2016).
24. M. Liao, C. Chaudhari, G. Qin, X. Yan, C. Kito, T. Suzuki, Y. Ohishi, M. Matsumoto, and T. Misumi, "Fabrication and characterization of a chalcogenide-tellurite composite microstructure fiber with high nonlinearity," Opt. Express **17**, 21608–21614 (2009).
25. S. Xie, F. Tani, J. C. Travers, P. Uebel, C. Caillaud, J. Troles, M. A. Schmidt, and P. S. Russell, "As_2S_3-silica double-nanospike waveguide for mid-infrared supercontinuum generation," Opt. Lett. **39**, 5216–5219 (2014).
26. S. P. Singh, V. Mishra, P. K. Datta, and S. K. Varshney, "Dispersion Engineered Capillary-Assisted Chalcogenide Optical Fiber Based Mid-IR Parametric Sources," J. Lightwave Technol. **33**, 55–61 (2015).
27. S. Shabahang, G. Tao, M. P. Marquez, H. Hu, T. R. Ensley, P. J. Delfyett, and A. F. Abouraddy, "Nonlinear characterization of robust multimaterial chalcogenide nanotapers for infrared supercontinuum generation," J. Opt. Soc. Am. B **31**, 450–457 (2014).
28. L. Shen, N. Healy, L. Xu, H. Y. Cheng, T. D. Day, J. H. V. Price, J. V. Badding, and A. C. Peacock, "Four-wave mixing and octave-spanning supercontinuum generation in a small core hydrogenated amorphous silicon fiber pumped in the mid-infrared." Opt. Lett. **39**, 5721–5724 (2014).

1. Motivation

Supercontinuum (SC) light sources rely on the nonlinear generation of new frequencies from an incident pulsed laser and can reach a spectral broadness of several hundreds of nanometers. Almost all practically relevant SC devices use optical fibers and are applied in a vast number of fields like medical imaging [1], metrology [2], or, single-shot spectroscopy [3]. Important recent development in the field includes octave spanning SG-generation (SCG) in the UV to near-IR [4] and in the mid-IR wavelength region [5]. SCG requires dispersion engineered waveguides [6], which allow the efficient light generation in desired spectral domains. To improve the generation performance in terms of brightness and broadness, two strategies are followed recently: (i) increasing the nonlinear response by incorporating materials with high nonlinear and linear refractive index (RI) into low RI claddings [7–10] or (ii) increasing the modal confinement using tapered fibers in which light is guided inside a freely suspended core [11, 12]. It is generally believed that the optimal conditions to achieve efficient SCG are those with a maximal possible confinement in the core, i.e. an as small as possible mode field diameter (MFD) [13, 14]. Mostly, this argument is rather used in a qualitative way with no in-depth study of its actual correctness. Strong modal confinement in high RI-contrast waveguides requires core diameters of the order or even below the operation wavelength. On such small dimensions the weak-guidance approximation commonly used to calculate nonlinear quantities becomes an invalid assumption, and the full vector character of the modes has to be taken into account. The corresponding numerics are time consuming and require solving Maxwell's equations by using time domain solvers. From the design point of view a straightforward-to-use design rule to estimate the optimal

Optics EXPRESS

waveguide parameters is highly desirable for conducting preliminary nonlinear calculations, thereby greatly reducing the calculation effort.

In case of step-index fibers (SIF) the used materials and the core diameter influence two key quantities, namely the nonlinear parameter γ and the group velocity dispersion (GVD). A lot of attention has been focused onto tailoring the GVD by designing microstructured silica fibers such as photonic crystal fibers [15]. Such fibers allow a wide tuning of the zero-dispersion-wavelength that sets the transition point from normalous (GVD < 0) to anomalous dispersion (GVD > 0), and, thus, selects the dominant nonlinear process for a given pump wavelength (e.g. four-wave-mixing or soliton fission). However, only little attention has been drawn to the nonlinear coefficient itself. For instance, the spectral distribution of the effective mode field area strongly effects the wavelength dependence of γ and is neglected in many studies. This rough approximation is effectively only valid for weakly guiding systems with small material dispersion and does not hold if high RI-contrast waveguides are considered.

Here we present a detailed numerical study on the properties of the nonlinear coefficient γ in the case of strongly confining fibers with sub-wavelength diameters (diameter smaller than the vacuum operation wavelength λ_0). The conducted study is independent of the actual value of the material nonlinearity n_2 and reveals the fundamental dependency of γ on wavelength, RI and core diameter. We introduce an accurate expression for the nonlinear coefficient in section 2 by taking into account the vector nature of the field for every core diameter. We additionally find an entirely analytic expression for the MFD, allowing us to reveal that the highest possible nonlinearity is in fact not correlated with the smallest MFD, but rather with the single-mode criterion, which is easily accessible via a well-known simple analytic expression. We discuss two relevant examples of highly nonlinear fiber waveguides, namely tapered fibers (section 3) and small-core step-index fibers (section 4), as depicted in Fig. 1(a). Finally, numerical limits and benefits are discussed (section 5).

2. Theoretical background

The nonlinear parameter γ describes the strength of the nonlinear response of the fiber and is one of the key quantities for many nonlinear phenomena such as soliton generation, self-phase modulation or four-wave-mixing [16]. A commonly used expression for the nonlinear coefficient is:

$$\gamma = k_0 n_2 / A_{\text{eff}} \tag{1}$$

with the vacuum wave vector k_0 ($k_0 = 2\pi/\lambda_0$), the nonlinear refractive index n_2, and the effective mode area A_{eff}, which is often approximated by a circular cross section of a Gaussian beam $\frac{\pi}{4} MFD^2$. The mode field diameter (MFD) is usually calculated using an intensity weight integral over area [13, 17]

$$MFD^2 = 8 \frac{\iint_\infty S_z r^3 \,\mathrm{d}r\mathrm{d}\varphi}{\iint_\infty S_z r \,\mathrm{d}r\mathrm{d}\varphi} \tag{2}$$

with the radial and azimuthal coordinates r and φ. In the case of cylindrical step-index fibers the longitudinal component of the Poynting vector S_z has a mathematically analytical form [18]. Therefore and due to the r^2 in the nominator all integrals of Eq. (2) can be solved analytically, leading to an entirely analytical expression for the MFD (see Appendix B).

Equation (1) states that 3$^{\text{rd}}$ order nonlinear processes become more pronounced for tighter modal confinement. However, a double-lobe mode pattern and reduced intensity in the core can be observed if the diameter of the core falls below wavelength of the optical pump light (see Fig. 1(b)). In this case of strong mode confinement, the cladding contributes to the nonlinear parameter and Eq. (1) with the assumption $n_2 = n_2^{co}$ becomes inaccurate for calculating the nonlinear coefficient.

Optics EXPRESS

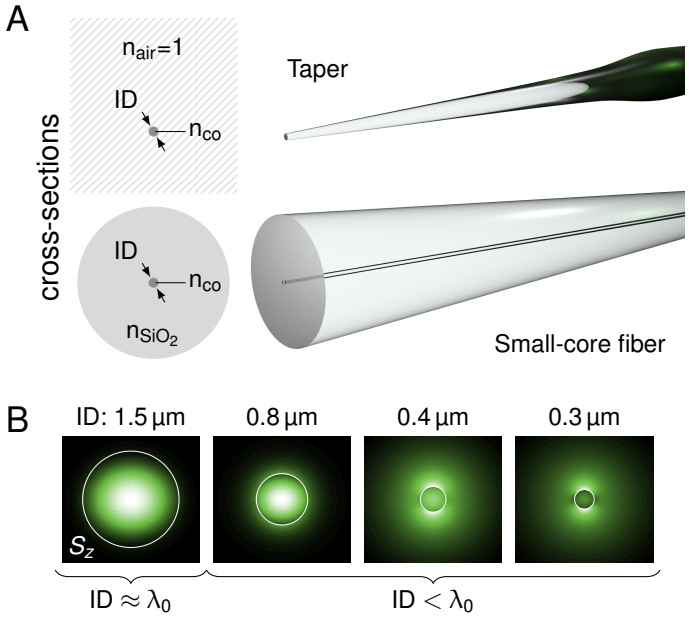

Fig. 1. (a) Cross sections and schematics of two nonlinear fiber structures discussed here: fiber taper in air and high RI-contrast step-index fiber. (b) Distributions of the Poynting vector (λ_0 = 1.55 µm) of a SiO_2 taper structure for four different core diameters (the number on the top of the images indicate the core diameter). The white circle indicates the core section.

There are mainly three definitions to calculate a more realistic γ which take into account the spectral dependence of the field components. The first definition relates to the weakly-guiding approximation and is given by the following expression [16]

$$\gamma^A = k_0 \frac{\iint_\infty n_2 |\mathbf{e}_\perp|^4 r\,\mathrm{d}r\mathrm{d}\varphi}{(\iint_\infty |\mathbf{e}_\perp|^2 r\,\mathrm{d}r\mathrm{d}\varphi)^2}\,. \tag{3}$$

In this model, the energy flow is defined via the absolute square of the transversal field components $\mathbf{e}_\perp$ being a weight by the nonlinear indices in core and cladding. This approach only holds in case of weakly guiding waveguides (i.e. small RI contrast). The second definition introduced by Foster *et al* [17] replaces $|\mathbf{e}_\perp|^2$ by intensity (see Eq. (5)), which is the longitudinal Poynting vector S_z. Both definitions do not include the longitudinal components of the electromagnetic field, since they are negligible in many situations. However, these components become prominent in wavelength-sized waveguides with strong index contrast. To take account for that, a rigorous derivation of γ was presented by Afshar and Monroe, which includes the entire electric vector field $\mathbf{e}$ [19]

$$\gamma^V = \frac{k_0 \varepsilon_0}{3\mu_0} \frac{\iint_\infty n^2 n_2 [2|\mathbf{e}|^4 + |\mathbf{e}^2|^2] r\,\mathrm{d}r\mathrm{d}\varphi}{|\iint_\infty S_z r\,\mathrm{d}r\mathrm{d}\varphi|^2} \tag{4}$$

with the linear refractive index n, the electric permittivity ε_0 and the electric permeability μ_0. We found that all three equations can be reduced to a semi-analytical equation with a one-dimensional integration over radius r for the case of a cylindrical step-index waveguide (see Appendix B for details).

Optics EXPRESS

Exemplarily, we demonstrate the solution pathway for the Foster definition [17] here. For a step-index waveguide, the integrals can be split in a core and a cladding contribution

$$\gamma = k_0 \frac{\iint_\infty n_2 S_z^2 r \,\mathrm{d}r\mathrm{d}\varphi}{(\iint_\infty S_z r \,\mathrm{d}r\mathrm{d}\varphi)^2} = k_0 \frac{n_2^{co} \iint_{co} S_z^2 r \,\mathrm{d}r\mathrm{d}\varphi + n_2^{cl} \iint_{cl} S_z^2 r \,\mathrm{d}r\mathrm{d}\varphi}{(\iint_\infty S_z r \,\mathrm{d}r\mathrm{d}\varphi)^2} \tag{5}$$

with the nonlinear RI of core n_2^{co} and cladding n_2^{cl}. Note that we neglect the superscript F on the Foster based γ and related quantities for simplicity. Considering only hybrid modes (Bessel order $m > 0$), the Poynting vector is composed of only three terms.

$$S_z = C_1 G_{m-1}^2(q) \; + \; C_2 G_{m+1}^2(q) + \; C_3 G_{m-1}(q) G_{m+1}(q) \cos(2m\varphi) \tag{6}$$

with the normalized transverse wave vectors q, the amplitude coefficients C_i and the general spheric functionals G_m (see Appendix B for details). Within the core one has $q_{co} = r(\varepsilon_{co} k_0^2 - \beta^2)^{1/2}$ and $G_m = J_m$, whereas $q_{cl} = r(\beta^2 - \varepsilon_{cl} k_0^2)^{1/2}$ and $G_m = K_m$ within the cladding with the respective material permittivities of core and cladding ε_{co} and ε_{cl}. The propagation constant β needs to be determined by semi-analytically solving the transcendental dispersion equation [18]. Thus, Eq. (5) can be rewritten into the following form

$$\gamma = k_0 \frac{n_2^{co} N^{co} + n_2^{cl} N^{cl}}{(D^{co} + D^{cl})^2} = A \cdot n_2^{co} + B \cdot n_2^{cl} = n_2^{co}(A + xB) \tag{7}$$

$$\text{with} \quad A = \frac{k_0 N^{co}}{(D^{co} + D^{cl})^2} \quad \text{and} \quad B = \frac{k_0 N^{cl}}{(D^{co} + D^{cl})^2} \tag{8}$$

with the ratio of nonlinear indices of core and cladding $x = n_2^{cl}/n_2^{co}$ and the core- and cladding-contribution factors A and B, respectively (for a detailed derivation see Appendix B). The latter two parameters solely depend on the geometry and on the used linear material RIs. The nominator and denominator parameters N and D in Eq. (7) are integrals over the radial coordinate within the respective material and are given by

$$N = 2\pi \int_\star^\star \mathrm{d}r \; r \Big[{C_1}^2 G_{m-1}^4(q) + {C_2}^2 G_{m+1}^4(q) + \left(\tfrac{1}{2}{C_3}^2 + 2C_1C_2\right) G_{m-1}^2(q) G_{m+1}^2(q) \Big], \tag{9}$$

$$D = 2\pi \int_\star^\star \mathrm{d}r \; r \Big[C_1 G_{m-1}^2(q) \; + \; C_2 G_{m+1}^2(q) \Big]. \tag{10}$$

The star symbols indicate the different integration domains (core: $[0, R]$, cladding: $[R, \infty]$, with R being the core radius). The D coefficients are entirely analytic. The N coefficients require a numerical integration along one dimension which, however, is a significant simplification of Eq. (5) compared to the usual two two-dimensional integrations.

Even though all presented equations are valid for $m > 0$, it is also possible to obtain the solution for the transversal electric (TE) and transversal magnetic (TM) modes ($m = 0$). For all mode types the explicit expressions of D and N can be found in Appendix B.

Analogously, γ^A (Eq. (3)) and γ^V (Eq. (4)) can be written in the same form with redefinitions of N and D, or A and B, respectively (see Appendix B). Thus, for all three definitions, it is possible to rewrite γ in a form similar to Eq. (1) with the distinction between effective mode field area in core and cladding: $\gamma = k_0 n_2^{co}/A_{\text{eff}}^{co} + k_0 n_2^{cl}/A_{\text{eff}}^{cl}$. The contribution factors A and B in Eq. (7) reveal the fundamental properties of cylindrical geometry in terms of nonlinear coefficient without requiring knowledge about the material nonlinearities and will be discussed in great detail in the next sections.

In the following we focus our discussion on the fundamental core mode ($m = 1$: HE_{11}) and discuss the characteristics of the core and cladding contribution factors A and B in the case of strongly confining tapers and hybrid multi-material fibers. Note that, although we concentrate the discussion on the quantities γ and A using the definition of Foster *et al*, we additionally present the other two definitions for a direct comparison and completeness.

Optics EXPRESS

3. Tapered fibers

Fiber tapers are thin cylindrical strands of homogenous glass in air with strand diameters of the order of a few micrometers or even below [11, 20, 21]. Due to the low nonlinearity of air, the nonlinear effects solely originates from the glass core with a practically negligible contribution from the cladding ($n_2^{co} \gg n_2^{cl}$). Thus, the cladding contribution term in Eq. (7) is negligible ($x \approx 0$) which allows the investigation of γ by studying exclusively the dependency of the core contribution factor A on structural parameters (radius and core RI) and wavelength.

For the first investigation (Fig. 2) we choose two fixed pump wavelengths at $\lambda_0 = 0.8\,\mu$m and 1.55 µm which are typical emission wavelengths of commercially available ultrafast lasers. For each value of core material (defined by the core RI n_{co}) a distinct maximum of the core contribution $A_{\max}^{n_{co}}$ (black dotted lines in Fig. 2) is observed for one particular core diameter d_{opt}. The maximum value $A_{\max}^{n_{co}}$ increases and shifts towards smaller core radii for larger core RIs as a result of increasing modal localization to the core. Finally, a highly nonlinear configuration can be associated with a maximum nonlinear coefficient γ at $A_{\max}^{n_{co}}$ defined by one particular set of n_{co} and d_{opt}. This point of highest nonlinearity does not vary much between the Foster and Afshar definition ($A_{\max}^{n_{co}}$ and $A_{\max}^{V,n_{co}}$) unlike the Agrawal definition ($A_{\max}^{A,n_{co}}$), which is slightly off the maximum. The actual value of the core contribution A using the Agrawal definition can be much smaller than those obtained by the Foster or Afshar definition.

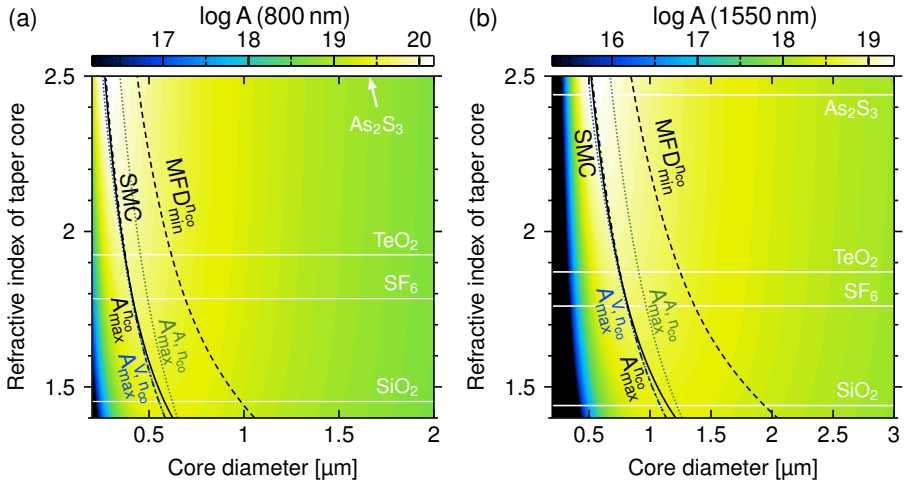

Fig. 2. Core contribution factor A (Foster definition, Eq. (5) and (7)) of the fundamental mode HE_{11} as function of core diameter and core RI in case of a fiber taper in air ($n_{cl} = 1$) for wavelengths (a) 800 nm and (b) 1550 nm. SMC: single-mode criterion ($V = 2.405$); $A_{\max}^{n_{co}}$: maximal core contribution at a fixed value of n_{co} (Foster: $A_{\max}^{n_{co}}$, Agrawal: $A_{\max}^{A,n_{co}}$, Afshar: $A_{\max}^{V,n_{co}}$); $\text{MFD}_{\min}^{n_{co}}$: minimal mode field diameter at fixed n_{co} (from Eq. (2)). The white horizontal lines indicate the material RIs of four selected core glasses: fused silica (SiO_2), lead-based SF6, tellurite (TeO_2) and chalcogenide glass (As_2S_3).

In general one can state that for a given core material (fixed RI) the core contribution $A^{n_{co}}$ decreases rapidly for core diameter different from d_{opt}. Especially, for smaller core diameter a non-intuitive drop-off appears, what can only be explained by investigating the mode field being pushed out of the core (example is shown in Fig. 1). However, low-RI cores are more robust against structural irregularities, which comes with the disadvantage of an overall lower nonlinear coefficient. In all selected cases (doped silica, lead-based SF6 glass, tellurite glass and non-oxide chalcogenide glass) the largest value of A requires deep sub-wavelength core

Optics EXPRESS

diameters. Remarkably, the silica taper reveals an only ten times smaller core contribution factor than the As_2S_3 system, even though the core/cladding RI contrast is substantially smaller.

From the design point of view, a practical rule for selecting the optimum core diameter for a given pump wavelength λ_0 and core index n_{co} is highly desirable instead of conducting extensive numerical calculations. In case of step-index waveguides one key expression is the single-mode criterion (SMC), generally separating the regions of single-mode and multi-mode operation. The single-mode criterion for cylindrical step-index fibers is defined by the V-parameter, $V = k_0 R(n_{co}^2 - n_{cl}^2)^{1/2}$, which has to be smaller than $V_{\mathrm{crit}} = 2.405$ for single-mode operation. We empirically found that the SMC (solid black line in Fig. 2) almost perfectly matches the optimum core contribution $A_{\mathrm{max}}^{n_{co}}$, especially for $n_{co} > 1.5$. As a consequence, the SMC accurately describes the location of $A_{\mathrm{max}}^{n_{co}}$, whereas the location of the smallest MFD ($\mathrm{MFD}_{\mathrm{min}}^{n_{co}}$, dashed black line in Fig. 2), which is generally considered as that point of strongest possible field confinement, fails to predict the optimum of A. This finding stands in strong contrast to the general believe that the mode with the highest localization gives the largest nonlinear response. Instead, the SMC appears to be an appropriate design tool not only for the modal operation regime, but also for optimizing the nonlinear response of fiber tapers. For a predefined core RI the taper radius at which the core contribution factor and thus the nonlinearity is approximately maximal is then given by:

$$d_{\mathrm{opt}} = 2R_{\mathrm{opt}} = 0.754\,\lambda_0 \cdot (n_{co}^2 - n_{cl}^2)^{-1/2}. \tag{11}$$

This expression only includes the core radius, the constituent material RI and the wavelength, making it straightforward to apply and extensive numerical calculations partially obsolete.

To verify that the SMC is a valuable tool to optimize taper designs in terms of nonlinearity, we investigate γ as function of pump wavelength and core diameter for two representative glass systems: SiO_2 and chalcogenide glass As_2S_3.

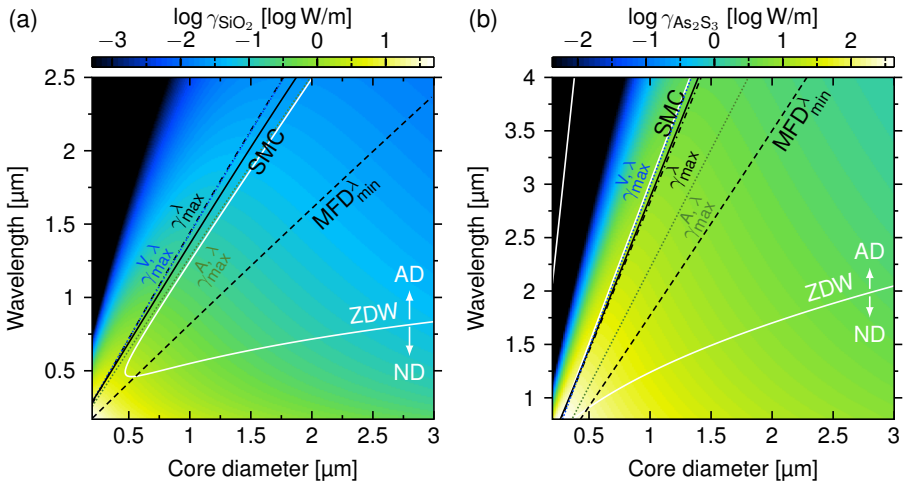

Fig. 3. Nonlinear coefficient (Foster definition, Eq. (5)) of a fiber taper in air as function of wavelength and core diameter for two representative glasses: (a) silica (SiO_2), (b) chalcogenide (As_2S_3). The color bar on the top refers to the decadic logarithms of γ. ZDW: zero dispersion wavelength, AD, ND: anomalous and normal dispersion, SMC: single mode criterion.

Starting with the silica taper (Fig. 3(a)), we assume that the nonlinear RI is wavelength-independent and has a constant value of $n_2 = 2.8 \times 10^{-20}\,\mathrm{m^2/W}$ [16]. This assumption holds if electronic resonances are spectrally far away, and we therefore limit our investigation to the

Optics EXPRESS

spectral domain 0.5 µm $< \lambda_0 <$ 2.5 µm, whereas the long-wavelength boundary is defined by the onset of strong vibrational absorption of silica. The region of highest γ values is located at small diameters and short wavelengths. A significant reduction of γ by several orders of magnitude is observed towards larger cores and longer wavelengths. The diameter at which γ is maximum for a given wavelength ($\gamma^{\lambda}_{\mathrm{max}}$) increases towards longer wavelengths and closely follows the evolution of the SMC for all three γ definitions. At any wavelength, both SMC and $\gamma^{\lambda}_{\mathrm{max}}$ are located in the anomalous dispersion region. This close correlation enables a fast estimation of the high nonlinearity regions in relation to the locations of the ZDW. In contrast, the point of highest mode localization i.e. smallest MFD (MFD$^{\lambda}_{\mathrm{min}}$ in Fig. 3(a)) is far off from $\gamma^{\lambda}_{\mathrm{max}}$ and, more specifically, falls in the opposite region of GVD.

An even better agreement between SMC and optimum $\gamma^{\lambda}_{\mathrm{max}}$ is achieved in the case of a chalcogenide taper (Fig. 3(b), here As_2S_3 [11], $n_2 = 2.92 \times 10^{-18}$ m^2/W). However, since the RI contrast is large the Agrawal model becomes to inaccurate to describe the location of highest γ, whereas the Foster and the Afshar definitions only slightly deviate from the SMC. Again, the SMC accurately resembles the evolution of $\gamma^{\lambda}_{\mathrm{max}}$ and lies in the same GVD regime. All findings show the importance of the SMC as a straightforward-to-use tool for optimized designs of fiber tapers in terms of nonlinearity and ZDW.

4. Highly nonlinear step-index fibers

In contrast to tapers, high-contrast step-index fibers (SIF) with highly nonlinear core materials and glass claddings provide several key advantages compared to tapers such as strong mechanical stability, splicability, and encapsulation of the core material, with the latter being important for hydroscopic or oxygen-sensitive glass systems [22, 23]. The most prominent cladding material is fused silica due to its high softening temperature, which enables filling of capillaries with the melt of different high-RI materials. Such systems led to a series of broadband SC sources emitting in the near and mid-IR wavelength region what has recently attracted strong attention [9, 24–28].

However, the glass cladding lowers the RI contrast between core and cladding and the modal confinement compared to fiber tapers. The nonlinear index of the cladding n_2^{cl} is non-zero and thus the contribution of the cladding parameter B has to be taken into account (Eq. (7): $x \neq 0$). Even though, in most cases the cladding contribution can still be neglected due to the following two reasons: (i) the core contribution A is significantly larger than B for almost all relevant combinations of core diameter and RI, and (ii) many high-RI core materials have a nonlinear index n_2 which is at least one order of magnitude larger than that of silica. These two arguments allow to separate the domain by the moderate limit $A = B$ whereby for bigger inner diameter and Δn (non-hatched area in Fig. 4) the approximation $B \approx 0$ is tolerable, and the core contribution factor A has to be considered only (for more details see Appendix A).

Here, we discuss the dependency of the nonlinear coefficient of SIFs on RI difference between core and silica glass cladding ($\Delta n = n_{co} - n_{cl}$) and core diameter for a fixed operation wavelength ($\lambda_0 = 1.55$ µm) (Fig. 4).

Similar to tapers, the core contribution A increases towards smaller core diameters until an optimal core diameter d_{opt} is reached. A further decrease of the diameter leads to a substantial drop-off of A, which results from the increase of evanescent field in the cladding. This effect becomes more distinct for larger Δn making the fabrication of high-contrast SIF with optimal design parameters (Δn, d_{opt}) more susceptible to deviations from the optimal core diameter. This susceptibility is, however, less pronounced compared to fiber tapers. The SMC follows the evolution $A^{\Delta n}_{\mathrm{max}}$ reasonably accurate with an increasing accuracy towards higher values of Δn (see Fig. 4(a)). Both curves lie within the region where A dominates the cladding contribution factor B even for low Δn, placing our assumption of $B \approx 0$ on solid grounds.

The agreement between $A^{\Delta n}_{\mathrm{max}}$ and the SMC is overall less accurate than in the case of fiber tapers, which we attribute to the reduced localization of the mode to the guiding core. This is

Optics EXPRESS

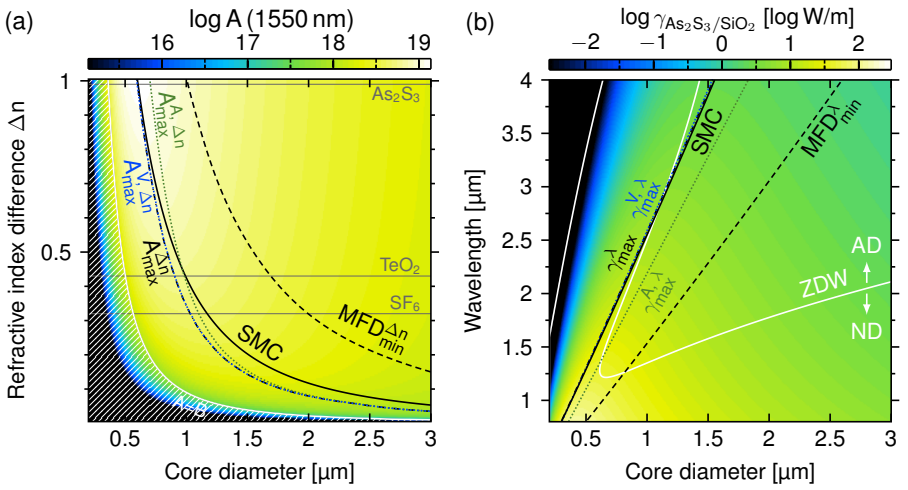

Fig. 4. (a) Core contribution factor A as function of core diameter and core-cladding RI difference Δn in case of a step-index fiber with fused silica cladding ($n_{cl} = 1.444$ at $\lambda_0 = 1.55\,\mu$m). SMC: single mode criterion; $A^{\Delta n}_{\max}$: maximal core contribution at a fixed value of Δn (Foster: $A^{n_{co}}_{\max}$, Agrawal: $A^{A,n_{co}}_{\max}$, Afshar: $A^{V,n_{co}}_{\max}$); $\mathrm{MFD}^{\Delta n}_{\min}$: minimum mode field diameter at fixed Δn; white patterned area: domain in which the cladding contribution dominates ($B > A$). The horizontal gray lines indicate the material RIs of three selected core glasses: lead-based SF6, tellurite (TeO_2) and chalcogenide glass (As_2S_3). (b) Nonlinear coefficient of a hybrid step-index fiber (As_2S_3 core, SiO_2 cladding) as a function of wavelength and core diameter. ZDW: zero dispersion wavelength; $\gamma^{\lambda}_{\max}$: maximum nonlinear coefficient per fixed wavelength. The colorbar refers to values based on the Foster definition (Eq. (5)).

also the reason for the difference in the location of highest core contribution factor between the three definitions ($A^{\Delta n}_{\max}$, $A^{A,\Delta n}_{\max}$, $A^{V,\Delta n}_{\max}$). However, the location of the minimal MFD ($\mathrm{MFD}^{\Delta n}_{\min}$) remains being far off from any definition of A. The optimal core diameter is again defined by the SMC via Eq. (11), which generally applies to all kinds of step-index fibers with cylindrical core and infinite extension of the cladding, since it originates from the corresponding definition of the V-parameter. Also note that large values of A require sub-wavelength core diameters similar to tapers - a behavior which is predicted by the MFD only for certain combinations of Δn and core diameters. This proves the $\mathrm{MFD}^{\lambda}_{\min}$ to be an inaccurate benchmark figure for optimizing the nonlinearity of small-core fibers.

An important SIF geometry which is currently under intense investigation is a hybrid design consisting of a chalcogenide core (here As_2S_3) and a fused silica cladding [9, 10, 25]. For this system the wavelength/diameter dependence of the maximum nonlinear coefficient ($\gamma^{\lambda}_{\max}$) is accurately resembled by the SMC (Fig. 4(b)), whereas the minimal MFD misleads again. Furthermore, the SMC predicts the location of the second ZDW which can be important for effects such as supercontinuum generation.

The MFD extends beyond the typically diameter of the step index fiber (125 µm) only in the domain of extremely small nonlinear parameter (referring to the situation where the cladding factor B dominates the core contribution factor A, black regions of Fig. 4(a)). Thus, the step-index approach with infinitely extended cladding used here is appropriate for any practically relevant nonlinear situation.

Optics EXPRESS

5. Numerical benefits and limits

By using an analytic form of the field components and the longitudinal Poynting vector [18] we found that the calculation for the nonlinear coefficient γ can be greatly simplified and substantially accelerated. Typically two-dimensional integrations over one quadrant of S_z and S_z^2 have to be conducted, requiring at least $2 \times M^2$ operations. Our approach just uses a single one-dimensional integration of a low-order Bessel functions without explicit calculation of the Poynting vector or the fields, reducing the number of operations to $M \times \log M$ (e.g., if $M = 1000$, our approach requires 10^3 times less mesh points). This greatly simplifies the calculation procedure and allows extensively large-scale parameter sweeps with substantially reduced computational effort. Especially, it enables the online determination of γ in more complex algorithms which find widespread application in ultrafast nonlinear optics, like e.g. nonlinear pulse propagation solvers for longitudinal varying waveguides.

Another benefit of our approach is the entirely analytic form of the MFD, which allows the fast calculation for a vast number of parameter combinations. The resulting straightforward-to-implement equation (see Appendix B) are useful for instance to optimize the launching efficiencies in high RI-contrast waveguides, which typically require extremely fine mesh discretization in the corresponding numerical two-dimensional simulations (e.g. chalcogenite nanospike [9]). The calculation scheme applies to all guided waveguide modes and generally gives more accurate results of the MFD than the weakly-guiding ansatz.

6. Conclusion

In this contribution we presented an in-depth study of the properties of the nonlinear coefficient and the mode field diameter of the fundamental mode in fiber tapers and multi-material hybrid fibers. By including an analytic form of the electromagnetic fields we derived quasi-analytic expressions for the nonlinear coefficient, reducing the simulation effort to a simple one-dimensional integration over well-known Bessel functions. We revealed that the design parameters for the maximum nonlinear coefficient are precisely predicted by the single-mode criterion and not by the minimum of the mode field diameter (i.e. the point of strongest localization of the mode inside the core), which is generally believed to be the point of highest confinement.

Our argumentation also holds for all three major definitions of the nonlinear parameter (Agrawal, Foster, Afshar). The Agrawal definition is the least accurate in terms of nonlinear core contribution and deviate from the single-mode criterion in particular for high RI contrast waveguides. The Foster and Afshar definitions, however, only slightly differ and in fact show that the SMC can be used to accurately describe the condition for highest γ. For example, neglecting the longitudinal field components (i.e. Foster definition) leads to a maximum amplitude deviation of $< 10\,\%$ compared to the Afshar definition considering a silicon strand in air ($n = 3.45$) (see i.e. [19]).

As a result, the SMC represents a straightforward-to-use and reliable tool to optimize highly nonlinear fibers making intense numerical calculations unnecessary. Our analysis gives a more accurate understanding of nonlinear fiber systems and will help to improve the efficiency of nonlinear devices such as supercontinuum or optical parametric light sources in the future, especially regarding fiber tapers and hybrid fibers.

Appendix A - Relation between core and cladding factor

The fraction between the core and cladding contribution A/B changes over several orders of magnitudes (Fig. 5). This enables the definition of areas where we are able to neglect one specific integration factor as example. We marked the isolines where A is 100 times larger than B, and

Optics EXPRESS

smaller than B in Fig. 5. This simplifies the calculation of γ to

$$\gamma = A \cdot n_2^{co} \quad \text{for} \quad \log\frac{A}{B} > 2 \tag{12}$$

$$\gamma = B \cdot n_2^{cl} \quad \text{for} \quad \log\frac{A}{B} < -2\,. \tag{13}$$

Between both limits both integral factors in Eq. (9) are necessary to obtain correct values of γ. However, the fraction of the nonlinear indices between core and cladding has to be considered as well. Thus, the overall contribution limits can be shifted towards the left side by choosing core materials with a nonlinearity several orders of magnitudes larger than that in the cladding. This keeps the core contribution factor A as the dominant nonlinear quantity for fiber design. Considering this, we chose the limit $A = B$ for our discussion in this paper, until which Eq. (12) is applicable.

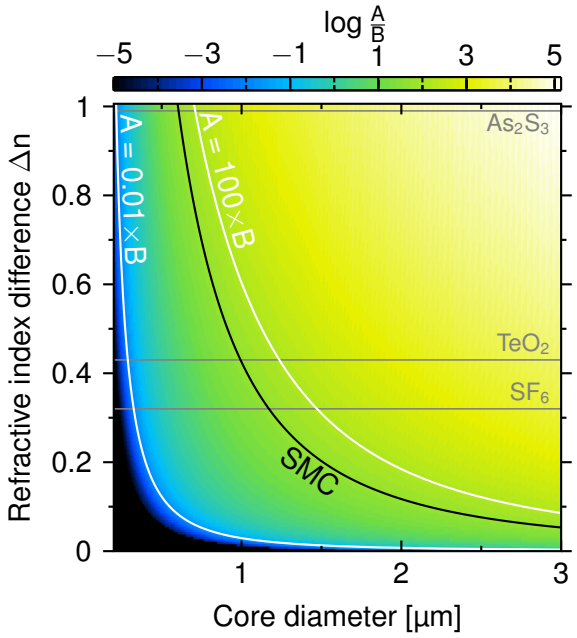

Fig. 5. Relation between core and cladding contribution A/B as function of the core diameter and the refractive index difference between core and cladding $\Delta n = n_{co} - n_{cl}$. This calculation was done for a fixed wavelength at 1.55 µm and fused silica as cladding material ($n_{cl} = 1.444$). Every value below $\log\frac{A}{B} = -5$ is clipped to remain sufficient image contrast. SMC: single-mode criterion; white solid lines: isolines for $\log\frac{A}{B} = \pm 2$; gray horizontal lines: refractive indices for three selected core materials: lead-based SF6, tellurite-based (TeO_2), and chalcogenide glass (As_2S_3).

Appendix B - Calculus

Nonlinear parameter by Foster

The following expression generalises the exact solution of the z-component of the Poynting vector S_z in a cylindrical core-cladding system [16]:

$$S_z = C_1\, G_{m-1}^2(q) \;+\; C_2\, G_{m+1}^2(q) + \; C_3\, G_{m-1}(q) G_{m+1}(q) \cos(2m\varphi)\,. \tag{14}$$

Optics EXPRESS

All functions, variables and constants are different in core and cladding (see table 1). Equation (14) is fully integrable over area and, thus, it is possible to find a semi-analytical expression for the definition of γ by Foster *et al* [17]. For that, we split the integrations over S_z into core and cladding domains with constant n_2:

$$\gamma^F = k_0 \frac{\iint_\infty n_2 S_z^2 r\,\mathrm{d}r\mathrm{d}\varphi}{(\iint_\infty S_z r\,\mathrm{d}r\mathrm{d}\varphi)^2} = \frac{2\pi}{\lambda}\frac{n_2^{co}N^{co} + n_2^{cl}N^{cl}}{(D^{co}+D^{cl})^2} \tag{15}$$

$$\text{with} \quad N = \int_0^{2\pi}\mathrm{d}\varphi \int_\star^\star \mathrm{d}r\; r S_z^2, \tag{16}$$

$$D = \int_0^{2\pi}\mathrm{d}\varphi \int_\star^\star \mathrm{d}r\; r S_z. \tag{17}$$

The stars of the second integral symbol indicate variable integration limits. The radial integration range is $[0,R]$ for the core (index *co*) and $[R,\infty]$ for the cladding (index *cl*). The azimuthal integration of S_z in Eq. (17) removes the last term of Eq. (14) and we find for the dominator integrals:

$$D = 2\pi \int_\star^\star \mathrm{d}r\; r(C_1\, G_{m-1}^2(q) \;+\; C_2\, G_{m+1}^2(q)) \tag{18}$$

$$\begin{aligned} &= 2\pi \left[\frac{C_1 r^2}{2}\left(G_{m-1}^2(q) - G_m(q)G_{m-2}(q)\right)\right]_\star^\star \\ &\quad + \; 2\pi \left[\frac{C_2 r^2}{2}\left(G_{m+1}^2(q) - G_m(q)G_{m+2}(q)\right)\right]_\star^\star . \end{aligned} \tag{19}$$

The stars have to be replaced by the integration limits as described before. Explicitly we get for core and cladding region:

$$D^{co} = \pi R^2 \left[C_1^{co}\left(J_{m-1}^2(U) - J_m(U)J_{m-2}(U)\right) + C_2^{co}\left(J_{m+1}^2(U) - J_m(U)J_{m+2}(U)\right)\right], \tag{20}$$

$$D^{cl} = -\pi R^2 \left[C_1^{cl}\left(K_{m-1}^2(W) - K_m(W)K_{m-2}(W)\right) - C_2^{cl}\left(K_{m+1}^2(W) - K_m(W)K_{m+2}(W)\right)\right]. \tag{21}$$

The numerator integrals does not break down so easily like the dominator. Solving the square of S_z in Eq. (16) results in

$$\begin{aligned} S_z^2 = {} & C_1^2 G_{m-1}^4 + C_2^2 G_{m+1}^4 + \left(C_3^2\cos^2(2m\varphi) + 2C_1C_2\right) G_{m-1}^2 G_{m+1}^2 \\ & + \left(2C_2C_3\; G_{m+1}^3 G_{m-1} + 2C_1C_2\; G_{m-1}^3 G_{m+1}\right)\cos(2m\varphi)\;. \end{aligned} \tag{22}$$

The angular integral removes the cosine term and leads to a factor π for the $\cos^2$ term. Thus, Eq. (16) becomes

$$N = 2\pi \int_\star^\star \mathrm{d}r\; r\left[C_1^2 G_{m-1}^4(q) + C_2^2 G_{m+1}^4(q) + \left(\tfrac{1}{2}C_3^2 + 2C_1C_2\right) G_{m-1}^2(q) G_{m+1}^2(q)\right]. \tag{23}$$

These terms cannot be solved analytically and have to be calculated numerically.

Nonlinear parameter by Agrawal

The definition of γ from the book of Agrawal [16] identifies the absolute square value of the transversal field components with the field intensity causing the nonlinear response. It is given as

Optics EXPRESS

follows

$$\gamma^A = k_0 \frac{\iint_\infty n_2 |\mathbf{e}_\perp|^4 r\,\mathrm{d}r\mathrm{d}\varphi}{(\iint_\infty |\mathbf{e}_\perp|^2 r\,\mathrm{d}r\mathrm{d}\varphi)^2} = \frac{2\pi}{\lambda_0} \frac{n_2^{co} N^{A,co} + n_2^{A,cl} N^{cl}}{(D^{A,co} + D^{A,cl})^2} \tag{24}$$

$$\text{with} \quad N^A = \int_0^{2\pi} \mathrm{d}\varphi \int_\star^\star \mathrm{d}r\; r |\mathbf{e}_\perp|^4, \tag{25}$$

$$D^A = \int_0^{2\pi} \mathrm{d}\varphi \int_\star^\star \mathrm{d}r\; r |\mathbf{e}_\perp|^2. \tag{26}$$

In case of cylindrical step-index geometries the transversal field components are analytic and their single and double squared absolute values have the following form:

$$|\mathbf{e}_\perp|^2 = |e_r(r)|^2 \begin{cases} \cos^2(m\varphi) \\ \sin^2(m\varphi) \end{cases} + |e_\varphi(r)|^2 \begin{cases} \sin^2(m\varphi) & \text{for } m \text{ even} \\ \cos^2(m\varphi) & \text{for } m \text{ odd} \end{cases} \tag{27}$$

$$\begin{aligned} |\mathbf{e}_\perp|^4 = {} & 2|e_r(r)|^2 |e_\varphi(r)|^2 \sin^2(m\varphi)\cos^2(m\varphi) \\ & + |e_r(r)|^4 \begin{cases} \cos^4(m\varphi) \\ \sin^4(m\varphi) \end{cases} + |e_\varphi(r)|^4 \begin{cases} \sin^4(m\varphi) & \text{for } m \text{ even} \\ \cos^4(m\varphi) & \text{for } m \text{ odd} \end{cases} . \end{aligned} \tag{28}$$

Using the electric field functions (e_r, e_φ, incl. radial field dependence) the dominator can be solved analytically

$$D^A = 2\pi \int_\star^\star \mathrm{d}r\; r(C_1 G_{m-1}^2(q) \; + \; C_2 G_{m+1}^2(q)) \tag{29}$$

$$\begin{aligned} & = \pi \left[C_1 r^2 \left(G_{m-1}^2(q) - G_m(q) G_{m-2}(q) \right) \right]_\star^\star \\ & \quad + \pi \left[C_2 r^2 \left(G_{m+1}^2(q) - G_m(q) G_{m+2}(q) \right) \right]_\star^\star . \end{aligned} \tag{30}$$

The star-symbols have to be replaced by the radial limits accordingly to core of cladding domain (see Foster definition). However, the nominator cannot be solved analytically and results in an expression which has to be integrated over the corresponding radial domain (indicated by the star-symbol)

$$N^A = 2\pi \int_\star^\star \mathrm{d}r\; r \left[C_1^2 G_{m-1}^4(q) + C_2^2 G_{m+1}^4(q) + 4 C_1 C_2 G_{m-1}^2(q) G_{m+1}^2(q) \right]. \tag{31}$$

All parameters can be found in Tables 1 and 2.

Nonlinear parameter by Afshar

The definition from Afshar and Monroe [19] derived an expression for the nonlinear parameter directly from Maxwell's equations. Despite its more complex appearance, we can rewrite it in a core and cladding contribution

$$\gamma^V = \frac{k_0 \varepsilon_0}{3\mu_0} \frac{\iint_\infty n^2 n_2 [2|\mathbf{e}|^4 + |\mathbf{e}^2|^2] r\,\mathrm{d}r\mathrm{d}\varphi}{|\iint_\infty S_z r\,\mathrm{d}r\mathrm{d}\varphi|^2} = \frac{2\pi\varepsilon_0}{3\mu_0 \lambda} \frac{n_{co}^2 n_2^{co} N^{V,co} + n_{cl}^2 n_2^{cl} N^{V,cl}}{(D^{co} + D^{cl})^2} \tag{32}$$

$$\text{with} \quad N^V = 2\pi \int_\star^\star \mathrm{d}r\; r \left[2|\mathbf{e}|^4 + |\mathbf{e}^2|^2 \right], \tag{33}$$

and with the dominator D defined in Eq. (17). Again, with the knowledge of the analytic expressions of all electric field components of a step-index fiber, the integral function in the

Optics EXPRESS

nominator can be expressed as

$$2|\mathbf{e}|^4+|\mathbf{e}^2|^2=3|\mathbf{e}_\perp|^4+3|e_z|^4\begin{cases}\cos^4(m\varphi)\\ \sin^4(m\varphi)\end{cases}\\ +2|e_z|^2e_\varphi^2\sin^2(m\varphi)\cos^2(m\varphi)+2|e_z|^2e_r^2\begin{cases}\cos^4(m\varphi) & \text{for } m \text{ even}\\ \sin^4(m\varphi) & \text{for } m \text{ odd}\end{cases} \tag{34}$$

Finally, the nominator can be expressed as a sum of the nominator from the Agrawal definition N^A (Eq. (31)) and a further radial integration. Here, the notation has to be distinguished between of hybrid HE/EH modes and transverse modes. For HE/EH modes we have

$$N^V=3N^A+2\pi\int_\star^\star \mathrm{d}r\, r\Big[\tfrac{9}{8}C_3^2G_m^4(q)\\ +C_3G_m^2(q)\left(C_1G_{m+1}^2(q)+C_2G_{m-1}^2(q)\pm\sqrt{C_1C_2}G_{m+1}(q)G_{m-1}(q)\right)\Big] \tag{35}$$

while for TE/TM modes we find

$$N^V=3N^A+2\pi\int_\star^\star \mathrm{d}r\, r\left[3C_3^2G_0^4(q)+2C_1C_3G_0^2(q)G_1^2(q)\right]. \tag{36}$$

All parameters can be found in Tables 1 and 2.

Mode field diameter

For the mode field diameter MFD, a fully analytical expression can be found. Therefore, we reformulate Eq. (2) to

$$MFD^2=8\frac{\bar{N}^{co}+\bar{N}^{cl}}{D_{co}+D_{cl}}\quad\text{with}\quad\bar{N}=\int_0^{2\pi}\mathrm{d}\varphi\int_\star^\star \mathrm{d}r\, r^3S_z, \tag{37}$$

and Eq. (17) for the D coefficients. Again, the azimuthal integral cancels the third term of S_z (Eq. (14)) and we obtain the following expression which has to be solved:

$$\bar{N}=2\pi\int_\star^\star \mathrm{d}r\, r^3\left(C_1G_{m-1}^2(q)+C_2G_{m+1}^2(q)\right). \tag{38}$$

The general solution for each integral term is given by

$$Z_m(x)=\int_\star^\star \mathrm{d}x\, x^3G_m(x)^2\\ =\tfrac{1}{3}x^2\left(\pm m(m-1)+\tfrac{1}{3}x^2\right)G_m(x)^2+\tfrac{1}{3}x^2\left(m^2-1\pm\tfrac{1}{3}x^2\right)G_{m+1}(x)^2\\ +\tfrac{1}{3}x\left(2m(1-m^2)\pm(1-m)x^2\right)G_m(x)G_{m+1}(x), \tag{39}$$

where the $\pm$ signs have to be chosen as $+$ for the core ($G_m=J_m$) and $-$ for the cladding ($G_m=K_m$) Using that we find the analytic solution for the $\bar{N}$ parameters

$$\bar{N}^{co}=\frac{2\pi R^4}{U^4}\left(C_1[Z_{m-1}^{co}(U)-Z_{m-1}^{co}(0)]+C_2[Z_{m+1}^{co}(U)-Z_{m+1}^{co}(0)]\right), \tag{40}$$

$$\bar{N}^{cl}=-\frac{2\pi R^4}{W^4}\left(C_1Z_{m-1}^{cl}(W)+C_2Z_{m+1}^{cl}(W)\right), \tag{41}$$

which enables with Eqs. (20) and (21) a fully analytical calculation of the MFD.

Constants and parameters

The nomenclature is based on a book by Snyder and Love [18].

Optics EXPRESS

Table 1. **Spatially dependent functions and constants**

	core	cladding
$G_m(q)$	$J_m(q)$	$K_m(q)$
q	$r(k_{co}^2-\beta^2)^{-\frac{1}{2}}$	$r(\beta^2-k_{cl}^2)^{-\frac{1}{2}}$
Agrawal/Afshar V.		
HE, EH modes		
C_1	$\frac{p}{4}\cdot(F_2-1)^2$	$\frac{p}{4}\cdot(F_2-1)^2$
C_2	$\frac{p}{4}\cdot(F_2+1)^2$	$\frac{p}{4}\cdot(F_2+1)^2$
C_3	$-pU^2/(R\beta)^2$	$-pW^2/(R\beta)^2$
p	$1/J_m^2(U)$	$U^2/W^2\cdot 1/K_m^2(W)$
TE modes		
C_1	0	0
C_2	$1/J_1^2(U)$	$1/K_1^2(W)$
C_3	0	0
TM modes		
C_1	$1/J_1^2(U)$	$n_{co}^2/n_{cl}^2\cdot 1/K_1^2(W)$
C_2	0	0
C_3	$-U^2/(R\beta J_1(U))^2$	$-n_{co}^2/n_{cl}^2\cdot W^2/(R\beta K_1(W))^2$

Foster		
HE, EH modes		
C_1	$\frac{p}{4}\cdot(F_1-1)(F_2-1)$	$\frac{p}{4}\cdot(F_2-1)(F_1-1+2\Delta)$
C_2	$\frac{p}{4}\cdot(F_1+1)(F_2+1)$	$\frac{p}{4}\cdot(F_2+1)(F_1+1-2\Delta)$
C_3	$(-1)^m\frac{p}{2}\cdot(1-F_1F_2)$	$(-1)^{m+1}\frac{p}{2}\cdot(1-2\delta-F_1F_2)$
p	$\alpha/J_m^2(U)$	$\alpha/K_m^2(W)\cdot U^2/W^2$
TE modes		
C_1, C_3	0	0
C_2	$\alpha/J_1^2(U)\cdot\beta^2/(k_0n_{co})^2$	$\alpha/K_1^2(W)\cdot\beta^2/(k_0n_{co})^2$
TM modes		
C_1, C_3	0	0
C_2	$\alpha/J_1^2(U)$	$1/(1-2\Delta)\cdot\alpha/K_1^2(W)$

Table 2. **Spatially independent constants.** A_m - modal amplitudes, R - core radius, $n_{co,cl}$ - refractive core/cladding index, β - propagation constant

α	$\lvert A_m\rvert^2 k_0 n_{co}^2/(2c_0\mu_0\beta)$		
F_1	$\left(\frac{UW}{V}\right)^2(b_1+(1-2\Delta)b_2)/m$	F_2	$\left(\frac{V}{UW}\right)^2 m/(b_1+b_2)$
b_1	$\frac{1}{2U}\left(\frac{J_{m-1}(U)}{J_m(U)}-\frac{J_{m+1}(U)}{J_m(U)}\right)$	b_2	$-\frac{1}{2W}\left(\frac{K_{m-1}(U)}{K_m(U)}+\frac{K_{m+1}(U)}{K_m(U)}\right)$
Δ	$\frac{1}{2}\left(1-n_{cl}^2/n_{co}^2\right)$	V	$R(k_{co}^2-k_{cl}^2)^{-\frac{1}{2}}$
U	$R(k_{co}^2-\beta^2)^{-\frac{1}{2}}$	W	$R(\beta^2-k_{cl}^2)^{-\frac{1}{2}}$

Acknowledgements

The authors acknowledge funding from the German Science Foundation (DFG) via the grants SCHM 2655/1-2 and SCHM 2655/3-1 and the Open Access fund of the Leibniz Association.